Thin Solid Films 518 (2010) 7245–7248

Contents lists available at ScienceDirect

Thin Solid Films

journal homepage: www.elsevier.com/locate/tsf

Preparation and characterization of ruthenium films via an electroless deposition route

Jing-Yu Chen, Li-Yeh Wang, Pu-Wei Wu *

Department of Materials Science and Engineering, National Chiao Tung University, Hsin-Chu 300, Taiwan, ROC

ARTICLE INFO

Available online 7 May 2010

Keywords:
Ruthenium
Ruthenium oxide
Electroless deposition

ABSTRACT

A metallic Ru film was prepared by an electroless deposition method, followed by hydrogen reduction treatment. The electroless deposition formulation produced a solid film on a Cu-coated Si substrate at 40 °C preactivated by $PdCl_2$ solution. Chemicals including $K_2RuCl_5 \cdot xH_2O$, $NaNO_2$, NaOH, and NaClO were mixed in a proper ratio that enabled heterogeneous nucleation and film growth. Results from X-ray photoelectron spectroscopy (XPS) on the as-deposited films confirmed the presence of RuO_x and Ru, while X-ray diffraction (XRD) pattern suggested an amorphous nature. Planar images from a scanning electron microscope revealed a rather smooth surface at thickness less than 250 nm. Above that formation of surface crack and partial detachment from the substrate were observed. After hydrogen reduction at 200 °C for 2 h, we obtained a metallic Ru film, as confirmed by XPS and XRD. In addition, the surface roughness was increased due to the formation of pinholes that was caused by the volume contraction associated with RuO_x reduction to Ru.

1. Introduction

In the family of platinum group metals (PGM), Ru is a relatively inexpensive element that exhibits low electrical resistivity and superb chemical stability. Hence, Ru has attracted significant attention recently for possible applications in electrocatalysis and semiconductor devices [1,2]. The oxidized form of Ru, RuO_x, is also of particular interest because of its unusually low electrical resistivity. For example, RuO_x is widely studied as the active material for pseudocapacitors, as well as electrocatalysis to promote the oxygen evolution reaction in a water electrolyzer [3,4].

To date, a variety of deposition methods have been explored to prepare Ru and RuO_x films. For example, vacuum-based approaches including physical vapor deposition, chemical vapor deposition, and atomic layer deposition have been demonstrated with various successes [5–7]. In general, these techniques involve expensive setups, long processing time, and excessive material waste. These drawbacks render them impractical to produce Ru and RuO_x films in a commercial scale. Therefore, considerable efforts have been devoted to identify an alternative route in solution-based depositions such as electroplating and sol–gel synthesis [8,9].

Electroplating is a known practice to fabricate films of metals and oxides [10]. However, to obtain a uniform deposit the substrate to be electroplated requires adequate electrical conductivity and simple surface contour. These criteria limit the applicability of electroplating to planar conductive substrates. In contrast, electroless deposition is able to operate on both conductive and insulating platforms in various shapes [11]. This is because the driving force for the electroless deposition comes from the reducing agent in the plating solution, which allows preferential nucleation and growth on the substrates. To date, among many metals derived from the electroless method, the Ni–P system has received the most scrutiny [12]. Typical steps for the electroless deposition entail substrate sensitization and activation, followed by electroless plating. Variables including pH, reducing agent, temperature, and additive are critical in determining the film qualities.

Among the PGM elements, the electroless depositions of Pd and Pt have been widely documented and their practices are rather common [10]. In contrast, there are much fewer studies on the remaining PGM metals including Ru, Os, Rh, and Ir [13,14]. Our experiences indicated that the electroless deposition for a solid Ru film is extremely challenging because in solution the Ru cation often exists in multiple oxidation states. As a result, possible disproportionation reactions would take place that renders homogeneous precipitation everywhere instead of desirable heterogeneous film growth on the substrate. In this work, we develop a practical Ru electroless deposition formulation and demonstrate the formation of Ru/RuO_x composite film on a Cu-coated Si substrate. After H_2 reduction, we convert the composite film to a crystalline Ru film.

2. Experimental details

An 8-inch Si wafer predeposited with SiO_2 (500 nm), TaN (20 nm), and Cu (60 nm) was used as the substrate. The wafer was broken into small pieces in $2 \times 2\ cm^2$, and rinsed with acetone and water to

* Corresponding author.
E-mail address: ppwu@mail.nctu.edu.tw (P.-W. Wu).

0040-6090/$ – see front matter © 2010 Elsevier B.V. All rights reserved.
doi:10.1016/j.tsf.2010.04.086

remove surface residues. Next, the sample underwent an activation treatment by submerging in an aqueous solution including 0.1 wt.% $PdCl_2$ (Aldrich) and 1 wt.% HCl (SHOWA) for 10 s. Subsequently, the activated substrate was immersed in the plating bath which contained 30 mL of aqueous solution consisting of 0.0186 g $K_2RuCl_5 \cdot xH_2O$ (Alfa Aesar), 0.0704 g $NaNO_2$ (SHOWA), 0.04 g NaOH (Mallinckrodt), and 1.8858 g NaClO (SHOWA). We carried out the electroless deposition at various times to estimate the deposition rate. Both the activation step and electroless deposition were conducted at 40 °C. Afterward, the sample was kept in the plating solution for 40 min and dried in air. To prepare a pure Ru film, we also performed a reduction treatment on the sample at 200 °C for 2 h in a mixture of 50% H_2 and 50% Ar.

The morphology and thickness for the as-deposited films were observed by a field emission scanning electron microscope (FESEM: JSM 6700). An atomic force microscope (AFM: Vecco Dimension 5000 Scanning Probe Microscopy) was used to determine their surface roughness. Phase and crystallinity for the samples were identified by a high-resolution X-ray diffractometer (HRXRD: Bede D1). The oxidation states of Ru and O were confirmed by an X-ray photoelectron spectrometer (XPS: Thermo Microlab 350).

3. Results and discussion

The electroless formation of Ru nanoparticles is very straightforward provided suitable reducing agents are employed. Unfortunately, due to the presence of multiple oxidation states for the Ru cations, it becomes rather challenging to deposit a continuous Ru film via the electroless route. To achieve preferential growth of Ru on the activated substrate, we designed a chemical bath with both reducer and oxidizer. In our formulation, the $K_2RuCl_5 \cdot xH_2O$ provided the source for Ru^{3+} cation while the $NaNO_2$ acted as the reducing agent. Because the $NaNO_2$ was unable to reduce Ru^{3+} directly, we adopted an indirect route in which the NaClO was added in the presence of NaOH to oxidize the Ru precursor to RuO_4. Subsequently, RuO_4 was reduced by the $NaNO_2$ to Ru and RuO_x, respectively. The thickness for the as-deposited film at various times is provided in Fig. 1. As shown, the deposit thickness grew faster at the beginning but became slower at a later stage. This behavior is expected as available Ru ions in the plating bath decreased with time.

To verify the chemical nature for the deposits, we employed XPS to determine the oxidation states for Ru and O. To obtain sufficient signal strength, we selected the sample after 480 min of electroless deposition. Fig. 2(a) displays the XPS profiles for the Ru $3p_{3/2}$ before and after hydrogen reduction. Although the Ru 3d signals are the strongest in XPS response, the binding energies for the metallic Ru and oxidized Ru are close to each other. Hence, it is difficult to determine the exact oxidation state for the Ru in the as-deposited film. Therefore, we decided to adopt the Ru 3p signals because they provided a better distinction between Ru and oxidized Ru. The other reason for not using the Ru 3d signals was to minimize possible interference from carbon. From the XPS profiles, apparently, the as-deposited film revealed a strong peak at 464.2 eV, confirming the presence of Ru. However, its position was slightly shifted relative to the metallic Ru at 462.2 eV [15], which suggested that the Ru existed both at metallic and oxidized states. Moreover, XPS results from the as-deposited films at various plating times demonstrated negligible variation, indicating reasonable consistence in the film composition. On the other hand, after hydrogen reduction the peak position was located at 462.7 eV. This inferred that a metallic Ru state was obtained. According to Matsui et al., in a hydrogen atmosphere, 200 °C was adequate to reduce RuO_x to Ru [16]. This substantiates our XPS results of Ru formation after hydrogen reduction.

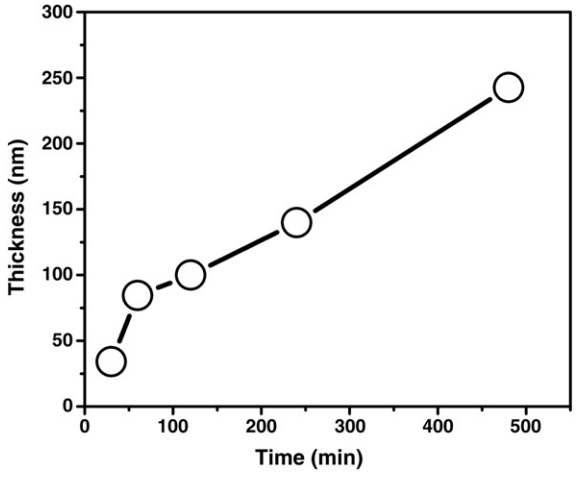

Fig. 1. Thickness variation for the as-deposited film as a function of plating time.

Fig. 2(b) provides the XPS profiles from O 1s signal on identical samples. As shown, before hydrogen treatment the peak position was 531.2 eV. From the XPS database, the O from RuO_2 and H_2O was expected to be 529.4 and 533.3 eV, respectively [15]. Hence, our signals inferred that Ru was likely in a hydrous form. This possibility was also suggested by Chang and Hu when they determined the O 1s signal from Ru–OH at 531.2 eV [17]. Interestingly, the O 1s signal after hydrogen reduction exhibited a slight shift to 532.1 eV, a value closer to what appeared to be surface H_2O. These evidences agreed well with those from the Ru $3p_{3/2}$, indicating that the reduction of RuO_x to Ru was achieved. We did not perform XPS curve fitting for O 1s signal because the oxygen can exist in states of RuO_x, adsorbed H_2O, and hydrated RuO_x. Previously, Shen et al. discussed similar issues and determined that the O 1s is difficult to assign [18]. In addition, the adsorbed H_2O can still be detected for the film after H_2 reduction. As a result, the O 1s signal was shifted less than 1 eV after H_2 reduction.

Fig. 3 presents the XRD patterns for the substrate, as well as films before and after hydrogen reduction. As shown, the as-deposited film revealed a broad peak from 30 to 40° amid considerable background noises. However, this pattern is inconsistent with those from standard diffraction patterns of Ru (JCPDS: 060663) and RuO_2 (JCPDS: 401290) but agreed well with that of the substrate. Hence, we surmised that the as-deposition film was amorphous in nature. In contrast, the XRD pattern after hydrogen reduction exhibited notable diffraction peaks and they were identified from the metallic Ru at 38° (100), 42° (002), and 44° (101), respectively. Similarly, those minor peaks between 30 and 40° were attributed to the Si substrate. However, we realized that the crystallinity for the Ru film was compromised moderately judging from the broad and relatively noisy background.

At this stage, evidences from XPS and XRD indicated that we deposited an amorphous Ru/RuO_x composite film and it was converted to a metallic Ru film after hydrogen reduction. Fig. 4 presents the SEM images in planar view for the as-deposited Ru/RuO_x films. As shown in Fig. 4(a), the Ru/RuO_x film after 120 min of electroless deposition revealed a smooth morphology with a thickness of 100 nm. In addition, there was presence of minute particles on the surface. In our SEM observations, the as-deposited films maintained reasonable surface uniformity within 240 min of deposition time. Above that, we noticed minor cracks around surface protrusions, and those cracks grew larger at increasing plating time. At 480 min, the film was broken into smaller pieces detaching from each other, as shown in Fig. 4(b). According to Chen et al. [19], the development of internal stress for a deposit during electroless deposition is attributed to both extrinsic and intrinsic factors. The extrinsic stress is known as “thermal stress” and it is associated with a mismatch in thermal expansion coefficient between the substrate and deposit. In contrast, the intrinsic stress is attributed to the processing parameters that lead to microstructural inhomogeneity such as grain boundaries, vacancies, and voids. Since the as-deposited films were

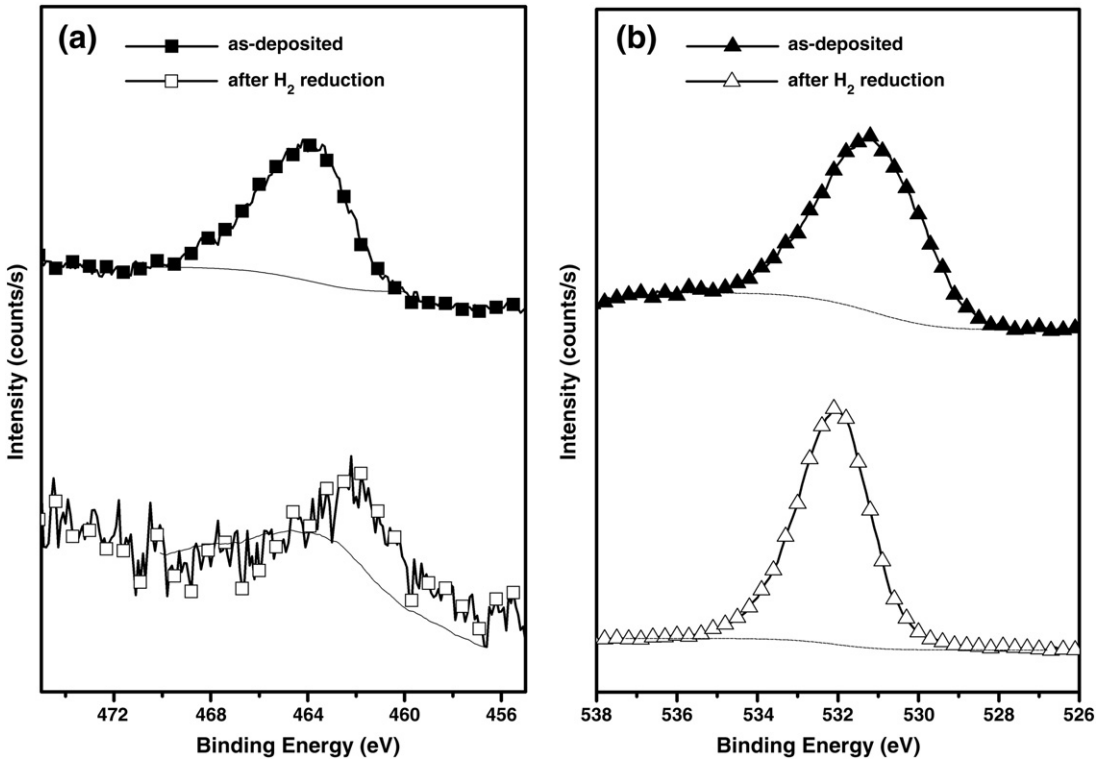

Fig. 2. XPS spectra for (a) Ru $3p_{3/2}$ line obtained from the as-deposited film and after hydrogen reduction, and (b) O 1s line from the same film before and after hydrogen reduction.

amorphous mixture of Ru and RuO_x, the presence of vacancies and voids was certainly possible to produce film cracking. On the other hand, thermal stress was not considered to be a factor because we performed the electroless deposition at 40 °C and the as-deposited film was cooled to room temperature slowly. Lastly, the lattice parameter mismatch between the deposit and substrate was unlikely to produce film cracks because the as-deposit film revealed an amorphous mixture.

The SEM images for the Ru films after hydrogen reduction are provided in Fig. 5. The sample in Fig. 5(a) was obtained from 120 min of electroless deposition and 2 h of hydrogen reduction. Clearly, there appeared many pinholes on the surface but the film still maintained its integrity. We understood that the conversion of RuO_x to Ru involved considerable volume contraction that might be responsible

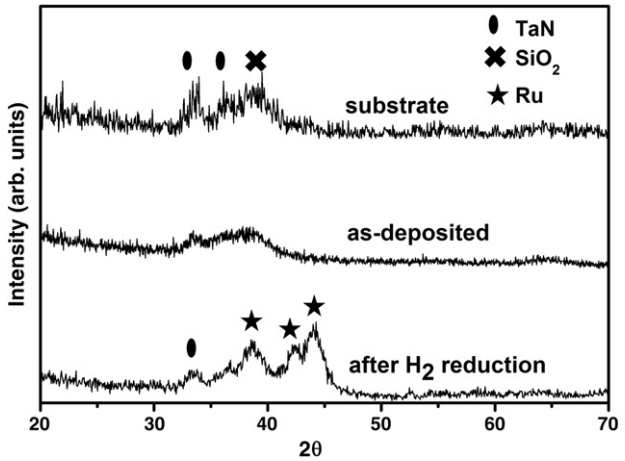

Fig. 3. XRD patterns for the substrate, as-deposited film after 480 min electroless deposition, and the same film after hydrogen reduction at 200 °C for 2 h.

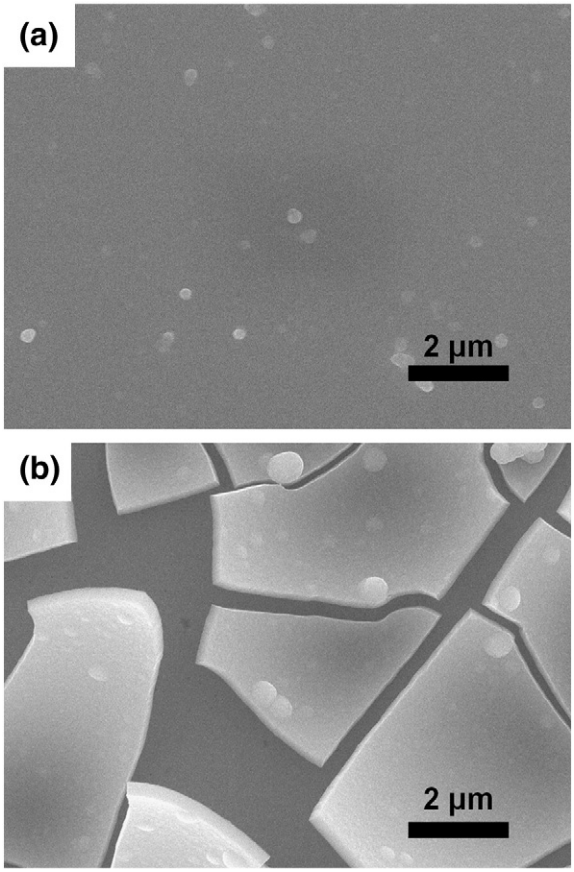

Fig. 4. SEM images in plain view for the Ru/RuO_x films after (a) 120 and (b) 480 min of electroless deposition.

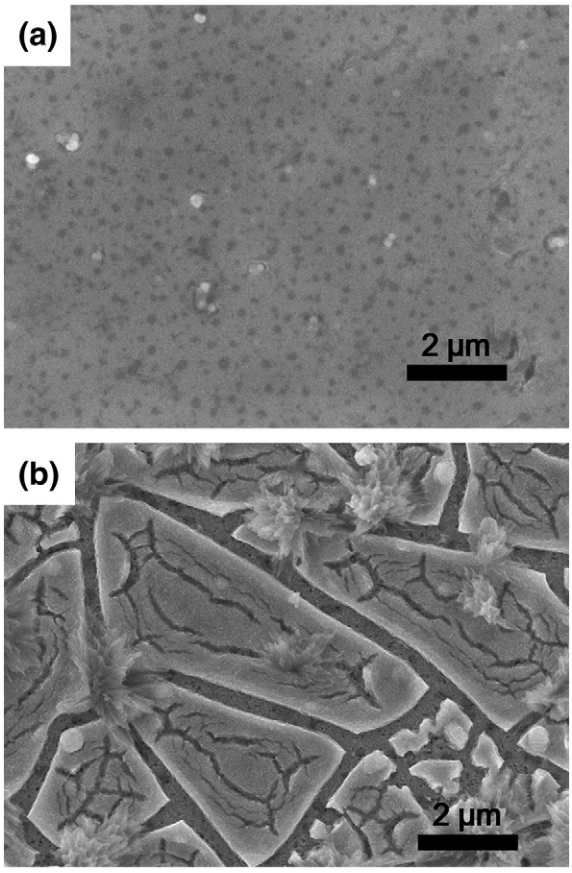

Fig. 5. SEM images in plain view for the Ru films obtained after (a) 120 and (b) 480 min of electroless deposition followed by hydrogen reduction at 200 °C for 2 h.

for the observed pinholes. As expected, when the plating time was increased, the number of surface pinholes in the reduced film was increased as well. In addition, we also witnessed the increase of surface roughness after the hydrogen treatment. The roughness value (R_q) from AFM for the as-deposited film was 4.59 nm, and it became 14.85 nm after hydrogen reduction. Fig. 5(b) displays the image from the sample of 480 min electroless deposition and 2 h hydrogen reduction. Apparently, there were severe structural alterations on the surface with protrusion of crystallites and cracks that penetrated to the substrate. This might explain the substantial noises recorded in earlier XRD and XPS analysis.

4. Conclusions

A composite Ru/RuO_x film was prepared on a Cu-coated Si substrate by an electroless deposition method in which activation and electroless plating were carried out consecutively at 40 °C. The plating bath contained chemicals including $K_2RuCl_5 \cdot xH_2O$, $NaNO_2$, NaOH, and NaClO that enabled heterogeneous nucleation and film growth on the activated substrate. Results from XPS and XRD on the as-deposited films confirmed the presence of RuO_x and Ru in an amorphous structure. The images from SEM indicated a solid film with smooth surface at thickness below 250 nm. Above that, surface cracking was observed that lead to film detachment from the substrate. After hydrogen reduction at 200 °C for 2 h, we obtained a metallic Ru film with surface pinholes caused by volume contraction associated with RuO_x reduction.

Acknowledgment

Financial support from the National Science Council of Taiwan (NSC 98-2221-E-009-040-MY2) is greatly appreciated.

References

[1] J.S. Spendelow, A. Wieckowski, Phys Chem Chem Phys 6 (22) (2004) 5094.
[2] S.K. Cho, S.K. Kim, H. Han, J.J. Kim, S.M. Oh, J Vac Sci 22 (6) (2004) 2649.
[3] J.H. Kim, D.S. Kil, S.J. Yeom, J.S. Roh, N.J. Kwak, J.W. Kim, Appl Phys Lett 91 (5) (2007) 052908.
[4] H.C. Ma, C.P. Liu, J.H. Liao, Y. Su, X.Z. Xue, W. Xing, J Mol Catal A Chem 247 (1-2) (2006) 7.
[5] J.G. Lee, Y.T. Kim, S.K. Min, S.H. Choh, J Appl Phys 77 (10) (1995) 5473.
[6] J.H. Shin, A. Waheed, W.A. Winkenwerder, H.W. Kim, K. Agapiou, R.A. Jones, G.S. Hwang, J.G. Ekerdt, Thin Solid Films 515 (13) (2007) 5298.
[7] S.K. Kim, S.Y. Lee, S.W. Lee, G.W. Hwang, C.S. Hwang, J.W. Lee, J. Jeong, J Electrochem Soc 154 (2) (2007) D95.
[8] Y.H. Lee, J.G. Oh, H.S. Oh, H. Kim, Electrochem Commun 10 (7) (2008) 1035.
[9] Y.S. Kim, H.I. Kim, J.H. Cho, H.K. Seo, G.S. Kim, S.G. Ansari, G. Khang, J.J. Senkevich, H.S. Shin, Electrochim Acta 51 (25) (2006) 5445.
[10] M. Paunovic, M. Schlesinger, R. Weil, in: M. Schlesinger, M. Paunovic (Eds.), Modern Electroplating, John Wiley & Sons, New York, 2000, p. 1.
[11] H. Matsubara, T. Yonekawa, Y. Ishino, N. Saito, H. Nishiyama, Y. Inoue, Electrochim Acta 52 (2) (2006) 402.
[12] K.I. Popov, S.S. Djokic, B.N. Grgur, Kluwer Academic/Plenum Publishers, New York, 2002.
[13] Y. Okinaka, C. Wolowodiuk, in: G.O. Mallory, J.B. Hajdu (Eds.), Electroless Plating : Fundamentals and Applications, American Electroplaters and Surface Finishers Society, Orlando, Fla, 1990, p. 421.
[14] C.R.K. Rao, D.C. Trivedi, Coord Chem Rev 249 (5-6) (2005) 613.
[15] NIST X-ray Photoelectron Spectroscopy Database, Version 3.5 (National Institute of Standards and Technology, Gaithersburg, 2003); http://srdata.nist.gov/xps
[16] Y. Matsui, M. Hiratani, S. Kimura, J Mater Sci 35 (16) (2000) 4093.
[17] K.H. Chang, C.C. Hu, J Electrochem Soc 151 (7) (2004) A958.
[18] J.Y. Shen, A. Adnot, S. Kaliaguine, Appl Surf Sci 51 (1–2) (1991) 47.
[19] Z. Chen, X.D. Xu, C.C. Wong, S. Mhaisalkar, Surf Coat Technol 167 (2-3) (2003) 170.